Visualizing the supersonic flow around a microvortex generator

F.K. Lu, A.P. Pierce, P.J. Gonzalez, and Y. Shih

1 Introduction

Microvortex generators (MVGs) have been proposed as devices for alleviating the adverse effects of shock/boundary-layer interactions [1]. MVGs in supersonic flow are generally skewed tetrahedral protuberances whose height is less than the boundary layer thickness (Fig. 1). Anderson et al. [1] provided MVG design guidelines, such as the standoff distance from an MVG array to the shock impingement location.

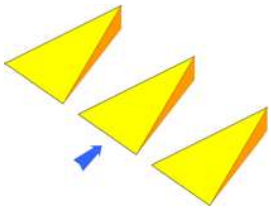

Fig. 1 Schematic of MVGs.

The physical mechanisms of how the MVG affects SBLI remain to be understood. With MVGs being lower than the boundary layer thickness, the concept of entrainment of the freestream into the boundary layer by a trailing vortex from each side of the MVG may need reexamination. Li and Liu [2], in their high-order large eddy simulations, revealed flow structures around an MVG that appear similar to those of Blinde et al. [3]. Blinde et al. suggested that a train of hairpin vortices is convected from the trailing edge of a MVG, while Li and Liu suggested a train of ring vortices; see Fig. 2. This paper reviews experimental visualizations that support most of Li and Liu's numerical observations.

2 Experimental Details

Experimental details can be found in [4] and only a brief description of the facility and visualizing techniques are provided here.

Aerodynamics Research Center, Mechanical and Aerospace Engineering Department, University of Texas at Arlington, Arlington, Texas 76019, USA

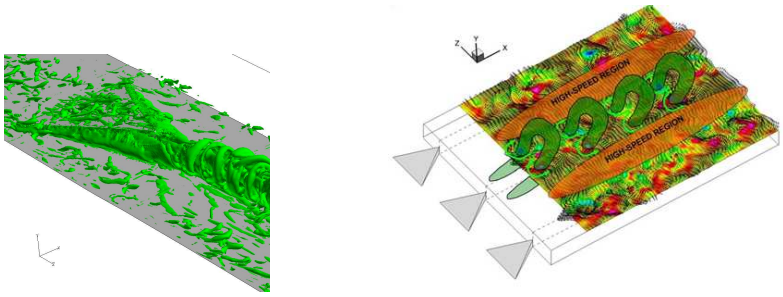

(a) Li and Liu's ring vortex train [2].

(b) Blinde's hairpin vortex train [3].

Fig. 2 Flow structure downstream of an MVG.

2.1 Facility

The experiments were performed in a blowdown wind tunnel at a Mach number of 2.47 ± 0.005. The tunnel operation was controlled by a host computer which opened the control valve to reach steady-state pressure conditions in 2–3 s. The total pressure was kept at 200 ± 6 kPa. The duration of the flow visualization experiments was less than 10 s long which resulted in a total temperature drop of only 1–2 K. Thus, despite the blowdown nature of the tunnel, the temperature can be considered to be steady for the present experiments. With the relatively steady total pressure and temperature, the unit Reynolds number can also be considered to be steady at 43 million/m.

Fig. 3 Test section with side wall removed to show flat plate. Flow from right to left.

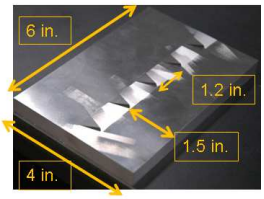

Fig. 4 Micro-vortex generator array.

The test section, shown in Fig. 3, was 15.2 cm^2 $\times$ 81.28 cm long. Extensive optical access was available from both sides and from the top. A flat plate, 73 cm long, with a 15-deg sharp leading edge was mounted in the test section. A turbulent boundary layer developed naturally over the top of the flat plate, with transition occurring within 3 cm from the leading edge. The boundary layer thickness was 3–4 mm in the test region.

Six MVGs in the form of skewed tetrahedra were distributed evenly across the flat plate such that their leading edges were located 272 mm downstream of the leading edge of the flat plate, Fig. 4. The MVGs were 12.95 mm long and 1.57 mm high. The front of each MVG was 11.7 mm wide. The center-to-center spacing between the MVGs was 30.5 mm. Two styles of MVGs were fabricated based on the designs of [2], with the trailing edge angle of either 45 or 70 deg. Flow visualizations of either MVG45 and MVG70 are qualitatively very similar.

2.2 Visualization Techniques

Three techniques were applied here, namely, surface flow visualization, laser lightsheet visualization and a new "panoramic" flow visualization. The surface flow visualization features a number of innovations, partly made possible by the extensive optical access [7]. Powdered fluorescent chalk of different colors in a mixture of kerosene and silicone oil was applied upstream of the test region. The bands of color that form during the run reveal the surface flow pattern under "blacklight." Lighting was introduced from both sides of the tunnel to prevent shadows. The images were acquired by cameras placed directly overhead. Other than the raw images, digital image processing was used to reveal inconspicuous features.

Laser lightsheet visualization was also straightforward. The arrangement in Fig. 5 shows the lightsheet aligned normal to the flat plate and in the streamwise direction. A spanwise arrangement was also used. Note that the laser lightsheet apparatuswas actually a stereo PIV system. Thus, the imaging was performed using one of the PIV cameras. Two different seeding methods were applied. The first utilizes 0.7 μm calcium carbonate particles (CalEssence70) injected into the stilling chamber of the wind tunnel. This method is called global lightsheet visualization. Figure 5 shows a local lightsheet arrangement where acetone was naturally aspirated into the boundary layer through a static port upstream of the interaction region. Subsequently, denatured alcohol, which is not corrosive to rubber seals, was also used effectively.

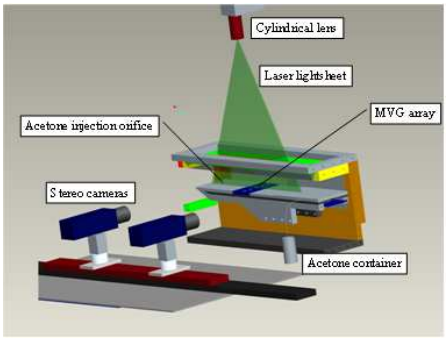

Fig. 5 Laser lightsheet arrangement.

Finally, instead of injecting vapor from one port, vapor was injected through three ports. Either acetone or alcohol was dyed which produced a colored vapor. The flow of the vapor across the MVG was imaged using a DSLR or a HD video camera. This method is called "panoramic" flow visualization.

3 Results and Discussion

An example of the surface flow visualization is shown in Fig. 6. The figure shows a small separation zone at the MVG leading edge even though the angle is less than that for incipient separation. This observation is put in context in Fig. 7 which plots the incipient ramp angle against the Mach and Reynolds numbers [9]. The figure includes data extracted from [10, 11]. It can be inferred that the incipient separation is due to the local transonic flow just ahead of the MVG and not the main supersonic flow. This small two-dimensional separation zone ahead of the MVG spills around

the side to produce a so-called open separation. Associated with this open separation is a pair of primary trailing vortices [2, 10, 11]. These vortices are different from a larger horseshoe vortex system that is extremely weak and not well observed.

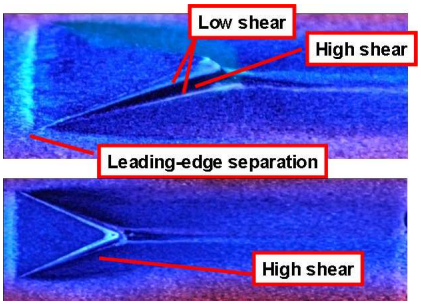

Fig. 6 Surface flow visualization showing open, three-dimensional separation.

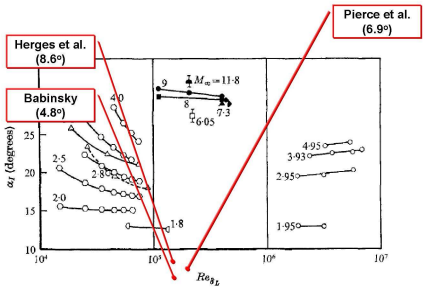

Fig. 7 Existence of separation ahead of MVG below the incipient separation threshold.

The open separation zone is marked by high shear with a dearth of pigment, both on the MVG side and on the flat plate, as indicated in Fig. 6. The high shear region on the MVG side is bounded by regions of low shear marked by accumulations of pigment. These low shear regions are required by topological rules [12] and are associated with secondary vortices emanating from the leading edge tips of the MVG. Topological rules also require the presence of vortex filaments at the leading-edge corners and at the rear of the MVGs although the rules do not stipulate the exact number. The visualizations thus far have not been able to resolve any vortex filaments along the leading-edge corners although vortex filaments have apparently been found. These latter vortex filaments will be discussed later.

A pair of streaks can be seen on the flat plate for a certain distance downstream of the MVG before disappearing. This disappearance has been attributed to the lifting of the primary vortex pair from the surface. However, such an interpretation may not be correct. A different interpretation is that the downstream flow is unstable with symmetry breaking [13]. To support this different interpretation, global lightsheet visualization reveals the presence of large flow structures downstream of the MVG trailing edge; see Fig. 8. Local lightsheet visualization of the flow over a flat plate and downstream of an MVG further reveals the presence of large flow structures in the latter. The suggestion here is that these structures are similar to those observed by Li and Liu [2] and Blinde [3] (Fig. 2).

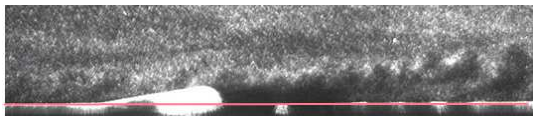

Fig. 8 Global lightsheet visualization showing presence of large structures downstream of the MVG trailing edge.

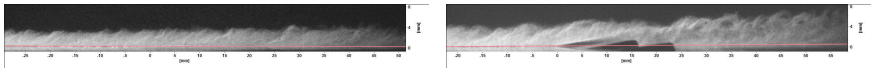

(a) Flat plate.

(b) With MVG showing large flow structures.

Fig. 9 Local lightsheet visualization.

It was remarked above that there is evidence to support the presence of vortex filaments at the vicinity of the rear tip of the MVG. Image processing of surface flow visualization videos reveal the presence of two spots near the rear tip. A frame from the video is shown in Fig. 10. A separate panoramic visualization reveals the presence of filaments in the flowfield near the rear tip which are apparently related to the surface singularities. A frame showing these filmanents is shown in Fig. 11. This figure shows another filament leaving the top of the MVG rear. Separately, Fig. 12 which shows pigment accumulation at the top of the rear to support this contention that vortex filaments also stream off the top. These observations are summarized into a detailed vortex flowfield model shown in Fig. 13 [5].

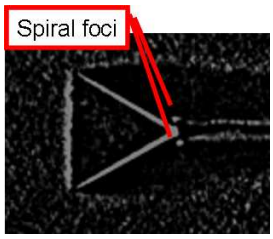

Fig. 10 Presence of a pair of singularities in surface flow visualization.

4 Conclusions

Creative use of accepted surface and flow visualizations, including the use of digital image processing, has effectively revealed numerous aspects of the complex flowfield around an MVG. Surface singularities and vortex filaments were revealed. The visualizations allowed a flowfield model to be developed that satisfies topological rules. The visualizations also support a downstream flow model that consists of either a train of ring or hairpin vortices that form due to instabilities arising from the confluence of the two primary vortices from both sides of the MVG. A detailed vortex flowfield model is proposed based on these observations.

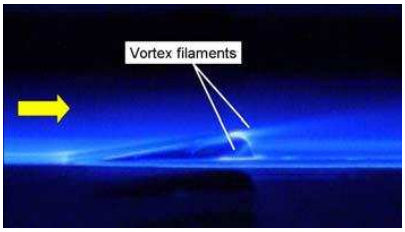

Fig. 11 Panoramic, near-surface visualization revealing vortex filaments.

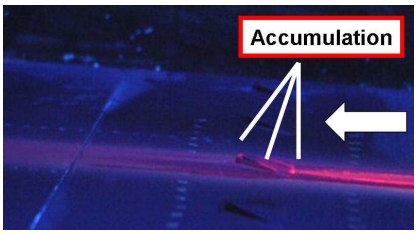

Fig. 12 Regions of pigment accumulation.

Acknowledgements
The authors gratefully acknowledge funding for this work via AFOSR Grant No. FA9550-08-1-0201 monitored by Dr. John Schmisseur. P.J.G. was supported by the Summer Louis Stokes Alliance for Minority Participation Program. The authors appreciate discussions with Prof. C. Liu and Dr. Q. Li.

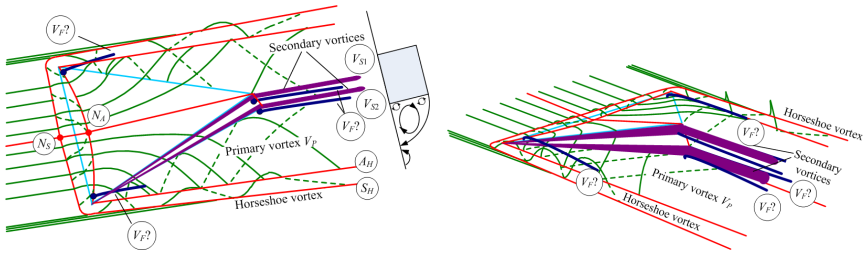

Fig. 13 The postulated mean flowfield topology past an MVG (dashed lines indicate surface flow). N_A, N_S = nodes of attachment and separation respectively; V_{S1}, V_{S2} = secondary vortices; S_H, A_H = separation and attachment associated with the horseshoe vortex; V_F = vortex filaments.

References

1. Anderson BH, Tinapple J, Sorber L (2006) Optimal Control of Shock Wave Turbulent Boundary Layer Interactions using Micro-Array Actuation. AIAA Paper 2006–3197
2. Li Q, Liu C (2010) Declining Angle Effects of the Trailing Edge of a Microramp Vortex Generator. J Aircraft 47(6):2086–2095.
3. Blinde PL, Humble RA, van Oudheusden BW, Scarano F (2009) Effect of Micro-Ramps on a Shock Wave/Turbulent Boundary Layer Interaction. Shock Waves 19(6):507–520.
4. Pierce AJ (2010) Experimental Study of Micro-Vortex Generators at Mach 2.5. MSAE thesis. Univ Texas Arlington.
5. Lu FK, Pierce AJ, Shih Y, Liu C, Li Q (2010a) Experimental and Numerical Study of Flow Topology Past Micro Vortex Generators. AIAA Paper 2010–4463.
6. Lu FK, Pierce AJ, Shih Y (2010b) Experimental Study of Near Wake of Micro Vortex Generators in Supersonic Flow. AIAA Paper 2010–4623.
7. Pierce AJ, Lu FK, Bryant DS, Shih Y (2010) New Developments in Surface Oil Flow Visualization. AIAA Paper 2010–4353.
8. Pierce AJ, Lu FK (2011) New Seeding and Surface Treatment Methods for Particle Image Velocimetry. AIAA Paper 2011–1164.
9. Elfstrom GM (1972) Turbulent Hypersonic Flow at a Wedge-Compression Corner. J Fluid Mech 53(1):113–127.
10. Babinsky H, Li Y, Pitt Ford C (2009) Microramp Control of Supersonic Oblique Shock-Wave/Boundary-Layer Interactions. AIAA J 47(3):668–675.
11. Herges T, Kroeker E, Elliott G, Dutton C (2010) Microramp Flow Control of Normal Shock/Boundary-Layer Interactions. AIAA J 48(11):2529–2542.
12. Tobak M, Peake DJ (1982) Topology of Three-Dimensional Separated Flows. Ann Rev Fluid Mech 14:61–85.
13. Crawford JD, Knobloch E (1991) Symmetry and Symmetry-Breaking Bifurcations in Fluid Dynamics. Ann Rev Fluid Mech 23:341–387.